Microstructural damage and repair in the spinal cord of patients with early multiple sclerosis and association with disability at 5 years

Malo Gaubert, Benoit Combès, Elise Bannier, Arthur Masson, Vivien Caron, Gaëlle Baudron, Jean-Christophe Ferré, Laure Michel, Emmanuelle Le Page, Bruno Stankoff, et al.

Microstructural damage and repair in the spinal cord of patients with early multiple sclerosis and association with disability at 5 years

Running Title

Spinal cord damage and repair in MS

Authors and affiliations

Malo Gaubert[1,2], Benoit Combès[2], Elise Bannier[1,2], Arthur Masson[2], Vivien Caron[2], Gaëlle Baudron[2], Jean-Christophe Ferré[1,2], Laure Michel[3], Emmanuelle Le Page[3], Bruno Stankoff[4,5], Gilles Edan[3], Benedetta Bodini[4,5] and Anne Kerbrat[2,3]

1 *Department of Neuroradiology, Rennes University Hospital, Rennes, France*

2 Empenn, INRIA, Rennes University- CNRS- INSERM, Rennes, France

3 Department of Neurology, Rennes University Hospital, Rennes, France

4 Paris Brain Institute (ICM), Sorbonne University- CNRS- INSERM, Paris, France

5 Neurology Department, APHP St Antoine Hospital, Paris, France

Abstract

Background and objective

The dynamics of microstructural spinal cord (SC)

damage and repair in people with multiple sclerosis (pwMS) and their clinical relevance have yet to be explored. We set out to describe patient-specific profiles of microstructural SC damage and change during the first year after MS diagnosis, and to investigate their associations with disability and SC atrophy at 5 years.

Methods

We performed a longitudinal monocentric cohort study among people with relapsing-remitting MS: first relapse < 1 year, no relapse < 1 month, and high initial severity on MRI (> 9 T2 lesions on brain MRI and/or initial myelitis). PwMS and age-matched healthy controls (HC) underwent cervical SC magnetisation transfer (MT) imaging at baseline, and at 1 year for pwMS. Based on HC data, SC MT ratio *z*-score maps were computed for each pwMS. An index of microstructural damage was calculated as the proportion of voxels classified as normal at baseline and identified as damaged after 1 year. Similarly, an index of repair was also calculated (voxels classified as damaged at baseline and as normal after 1 year). Linear models including these indices and disability or SC cross sectional area (CSA) change between baseline and 5 years were calculated.

Results

Thirty-seven patients and 19 HC were included. We observed considerable variability in the extent of microstructural SC damage at baseline (0-58% of SC voxels). We also observed

considerable variability in damage and repair indices over 1 year (0-31 % and 0-20%), with 18 patients showing predominance of damage, and 18 predominance of repair. The index of microstructural damage was associated positively with EDSS score (r = .504, p = .002) and negatively with CSA change (r = -.416, p = .02) at 5 years, independently of baseline SC lesion volume.

Discussion

People with early RRMS exhibited heterogeneous profiles of microstructural SC damage and repair. Progression of microstructural damage was associated with disability progression and SC atrophy 5 years later. These results indicate a potential for microstructural repair in the SC to prevent disability progression in pwMS.

Keywords

Multiple sclerosis, spinal cord, MRI, magnetisation transfer, remyelination, longitudinal

Introduction

Spinal cord (SC) lesions frequently occur in people with MS (pwMS),[1] and have a prognostic value early on the disease for the development of subsequent ambulatory disability.[2] However, in clinical practice, some pwMS have a high SC lesion load and a low level of disability, and vice-versa. One hypothesis is that patients have a different potential to remyelinate/demyelinate, which has an impact on the severity of their lesions. In contrast to the brain, the ability of the SC to remyelinate/demyelinate over time remains largely unexplored,[3,4] while degeneration of chronically demyelinated SC axons is considered to be the major pathological correlate of ambulatory disability.[5,6]

Complementing anatomopathological studies, the dynamic exploration of microstructural SC damage and repair in pwMS requires longitudinal studies using quantitative imaging. In particular, myelin PET imaging was used to describe the remyelination/demyelination profiles of pwMS over time.[7] To date, no myelin-specific PET studies have been carried out in the SC of pwMS, mainly owing to limited spatial resolution. Alternative MRI-based approaches can also be considered, such as magnetisation transfer (MT) imaging. This technique is less specific to myelin content than PET, but results have been shown to correlate well with both myelin and axonal tissue content.[8–10] In longitudinal brain MRI studies, it has been used to approximate microstructural variations at the voxel scale, both in white matter (WM)[11,12] and grey matter (GM).[13] To date, no such studies have been carried out at the SC level. More generally, studies involving longitudinal quantitative SC MRI acquisitions in pwMS remain scarce,[14–19] mainly owing to the technical challenges.[20]

Thus, the main objective of this pilot study was to describe patient-specific profiles of microstructural SC damage and repair during the first year after MS diagnosis. We investigated the associations between these profiles and disability and SC atrophy at 5 years.

Materials and methods

Standard Protocol Approvals, Registrations, and Patient Consents

All participants were enrolled in EMISEP, a multicentre longitudinal study approved by an institutional review board (NCT02117375)[21] and gave their written informed consent.

Study sample

The main inclusion criteria were i) diagnosis of relapsing-remitting MS (RRMS)[22] ii) first relapse < 1 year, iii) Expanded Disability Status Scale (EDSS) score < 3,[23] iv) age > 18 years, v) no relapse in month before inclusion, and vi) high severity on MRI (> 9 T2 lesions on brain MRI and/or initial myelitis on SC MRI). A group of healthy controls (HC) was matched for age with the pwMS group. The main inclusion criteria for HC were no family history of MS, and no central nervous system disease.

In the present study, we only included participants from the main inclusion centre (Rennes), owing to scanner variability between centres for MT ratio (MTR) measurement and too few HC for the other centres ($n < 5$) to compute *z*-score maps. The original dataset comprised 44 pwMS and 20 HC. Of these, seven pwMS and one HC had to be excluded from analyses, owing to comorbidity incompatible with disability assessment (one pwMS), missing MRI acquisition (one pwMS), issues during the acquisition protocol (two pwMS), or poor image quality (three pwMS and one HC). The final dataset therefore comprised 37 pwMS and 19 HC.

Clinical assessment

All participants were assessed by a senior neurologist every 6 months for 5 years, including the EDSS (and pyramidal subscale), Timed 25-Foot Walk (T25-FW), Six-Minutes Walk Test (6M-walk),[24,25] Nine-Hole Peg Test (9HPT),[25] 12-Item MS Walking Scale (MSWS-12),[26] and French-language version of the urinary disorder–specific quality of life questionnaire (Qualiveen).[27]

MRI acquisition

All participants underwent a baseline 3T MRI scan (Magnetom Verio, Siemens Healthineers, Erlangen, Germany, VB17) between January 2014 and April 2017 for pwMS and between March 2016 and December 2017 for HC. All pwMS had a second scan 12 months later on the same machine, and 36 had an MRI scan at 5 years on a different scanner of the same manufacturer (3T Magnetom Prisma). The acquisition protocol (detailed in eTable 1) was the same for all timepoints and was split into two consecutive sessions. The first one included T1-weighted (T1w) 3D MPRAGE imaging comprising brain and upper cervical SC and 3D FLAIR imaging with a 32-channel (64 for Prisma) head coil. The second one included SC acquisition with neck and spine coils: two sagittal T2-weighted (T2w) images covering the whole SC, T2*-weighted MEDIC (T2*w) axial images covering C1-C3 and C4-C7 SC vertebra levels, and two 3D gradient echo sequences with (MT1) and without (MT0) prepulse covering cervical SC and centred on C5 (manufacturer's default magnetization transfer prepulse [Gaussian envelope, 1200 Hz off-resonance frequency]). Only baseline and 12-month follow-up MT scans were considered for primary measures. The acquisitions at 5 years were used solely for secondary measures (CSA). The impact of the change of MRI scanner on CSA is discussed in eAppendix 1.

MRI processing

Processing was performed using the Spinal Cord Toolbox (SCT) v5.8 for the SC images,[28] FMRIB Software Library (FSL)[29] v6.0.5 and Anima v4.1[30] for brain and further processing.

Indices of microstructural change

Details of MTR computation are provided in eAppendix 2. Briefly, after rigid registration of the MT0 map to MT1 space, MTR maps were computed as the ratio of (MT0 - MT1) to MT0 (expressed as percentage), normalised to PAM50 template space[31] and smoothed with a ball kernel with 1-mm diameter. The full pipeline of processing from the baseline and 12-month follow-up MTR maps to the calculation of the indices is described in Figure 1. Cervical SC MTR values were taken as a proxy of microstructural integrity. Voxel-based *z*-score maps of MTR values at each timepoint (baseline and 12-month follow-up) for each pwMS were computed based on mean and standard deviation values calculated in the HC group. A similar voxel-based approach was previously used [7,12] and had the advantage to tackle the variability of the MTR measure associated with different SC locations.[21] In each pwMS at each time point, any given voxel with an MTR *z*-score more than 2.58 *SD*s below the mean (corresponding to a *p* value of .01) of the corresponding voxel in HC, was classified as having an abnormal microstructure. To confirm those results, all subsequent analyses were repeated with a thresholding of the MTR *z*-score maps at 1.96 *SD*s (corresponding to a *p* value of .05). Results are provided in eAppendix 3.

Three indices of microstructural content were then computed (Fig. 1C). First, an *index of dynamic microstructural damage* was defined as the percentage of voxels classified as damaged at 12-month follow-up but not at baseline. Second, an i*ndex of dynamic microstructural repair* was defined as the percentage of voxels classified as damaged at baseline but not at 12-month follow-up. Finally, a *global index of microstructural change*

was defined as the difference between these indices with positive values indicating predominant microstructural damage over the follow-up period, and negative values indicating repair. All three indices were computed for cervical SC (mask eroded by 1 mm, comprising C2-C6 from PAM atlas).

##########

 # Insert Figure 1

##########

Lesion segmentation

Cervical SC lesions were manually segmented on axial T2*w images as described elsewhere.[32] Details are provided in supplementary material (eMethods).[32]

Cross-sectional areas

The mean CSAs across C2 and C3 levels were computed on the T1w images at baseline and 5-year follow-up using the steps described in the SCT tutorial. As two different MRI scanners were used at baseline and at 5-year follow-up, we corrected for the variability induced by the change of machine (see eAppendix 1). The relative change between baseline and 5-year follow-up was computed as in Eq. (1).

$$\text{relative change} = \frac{[\text{mean CSA}_{\text{5-year}} - \text{mean CSA}_{\text{baseline}}] - [\text{mean CSA}_{\text{FU}} - \text{mean CSA}_{\text{BL}}]}{[\text{mean CSA}_{\text{FU}} + \text{mean CSA}_{\text{BL}}]} \quad (1)$$

Statistical analysis

All statistical analyses were performed using R v4.3.0 and RStudio 2022.07.2+576 with ppcor package (v1.1) for partial correlations and khroma (v1.12.0) and ggplot2 (v3.5.1) packages for data visualisation. First, we focused our analyses on microstructural abnormalities at baseline and at 12-month follow-up at the group level, to compare HC and

patients with RRMS. The mean signals for these group analyses were extracted in the C2-C6 mask. Second, we ran individual analyses to capture the uniqueness of the microstructural damage and repair profiles in patients over the 12-month follow-up. Third, we looked for associations between the indices and disability and SC atrophy 5 years later.

For all tests unrelated to the three microstructure indices, the significance threshold for results was set at $p < .05$. When considering analyses with the three microstructure-related indices, we used a significance level of $p < .0083$ (.05/6), corresponding to a Bonferroni correction for multiple comparisons. Age at baseline and sex were included as covariates in multiple regression models.

Baseline and 5-year follow-up characteristics

Differences in characteristics between the HC and pwMS groups were assessed using two-tailed two-sample *t* tests for continuous variables, and chi-squared (χ^2) tests for categorical variables. Two-tailed paired *t* tests were performed to assess changes in clinical and anatomical measures between baseline and 5-year follow-up data.

Microstructural damage at baseline

A two-tailed two-sample *t* test was computed to compare the pwMS and HC groups on MTR values for cervical SC at baseline. A partial linear correlation was computed with the percentage of abnormal voxels in cervical SC at baseline and lesion load at baseline (log-transformed in all subsequent analyses).

Microstructural damage and repair at 12-month follow-up

A two-tailed paired *t* test was used to assess the mean difference in MTR values between the two timepoints in the pwMS group. Individual profiles were then defined, based on our three indices. Finally, multiple regressions were computed between the three indices and T2*w

lesion load, percentage of microstructural abnormality at baseline, age at baseline, and sex at baseline, to assess the associations between these factors and microstructural change over time.

Microstructural damage and lesion location

We evaluated the location of microstructural damage cross-sectionally and longitudinally and the location of lesions at baseline in three different ways. First, regarding lesion locations, and microstructural damage at baseline and repair over time in GM or WM, we took the number of voxels for each index in each compartment (GM or WM) and divided it by the sum of voxels in GM and WM. Second, we computed percentages for each compartment by dividing the number of voxels for each index by the number of voxels in the whole cervical SC. For these two calculations, GM and WM in cervical SC were retrieved using the PAM50 atlas.[31] Third, the effect of distance from external cerebrospinal fluid (CSF) was assessed using a distance map computed with the *distancemap* tool provided by FSL and applied to the cervical SC mask (see above and illustration in Fig. 5). In each 0.5-mm thick ribbon, we computed the percentage of voxels in the ribbon with a lesion or microstructural damage at baseline or where microstructural damage or repair took place over time.

Associations with clinical and anatomical findings at 5-year follow-up

We ran three multiple regressions, one for each of the three indices of microstructural change as independent variables, and EDSS at 5-year follow-up as the dependent variable as in Eq. 2.

$$EDSS\ at\ 5\text{-}year\ follow\text{-}up = \beta_0 + \beta_1 * Index + \beta_2 * Age + \beta_3 * Sex + \varepsilon \quad (2)$$

With index = either Index of dynamic microstructural damage or Index of dynamic microstructural repair or Global index of microstructural change, β_0 the intercept, β_1, β_2, β_3 the regression coefficients and ε the error term.

The same model was applied with regards to CSA change between baseline and 5-year follow-up (Eq. (1)) as the dependent variable. Moreover, we conducted exploratory analyses with multiple regressions between the three indices as independent variables and the other clinical scores (i.e., pyramidal EDSS, T25-FW, 6M-walk, 9HPT, MSWS-12 and Qualiveen) as dependent variables (eTable 2). ANCOVAs were also computed to compare patients with versus without confirmed disability progression (defined as an increase in EDSS score of ≥1 point confirmed for at least 6 months and until the end of patient follow-up), with the three indices as independent variables. The T2*w lesion load at baseline and the presence (vs. absence; binary) of new lesions at 12-month follow-up (compared with baseline) were added as extra covariates for secondary analyses.

Data availability statement

Data supporting the findings of this study are available from the corresponding author, upon reasonable request.

Results

Baseline and follow-up characteristics

There was no significant change in clinical scores between 0 and 5 years at group level, except on the 9HPT (all *p*-values > .05, but 9HPT: $p < .001$; Table 1). Twelve out of 36 patients had confirmed disability progression during follow-up. CSAs were comparable across the HC and pwMS groups at baseline ($p = .166$), but greater at baseline than at 12-month follow-up in the pwMS group ($p < .001$).

######################

 # Insert Table 1

######################

Microstructural damage at baseline

Group-level analysis

MTR values in pwMS were lower than those of HC in both the whole cervical SC (HC: 35.672 ± 0.888 pu; pwMS: 34.649 ± 2.208 pu; $p = .017$; Cohen's d = 0.539) and, albeit to a lesser extent, in normal appearing cervical SC (pwMS: 34.938 ± 1.936 pu; $p = .058$; Cohen's d = 0.436).

Individual-level analysis

The percentage of microstructural damage in cervical SC varied considerably, ranging from 0 to 58% (see Fig. 2 for examples of pwMS with different degrees of baseline microstructural SC damage). A moderate positive association was observed between the SC lesion load

delineated on axial T2*w and the percentage of microstructural damage in cervical SC on MTR maps (r = .405, p = .016). However, the mean volume of lesions on T2*w (191.902 ± 319.274 mm^3) was much smaller than the volume categorised as damaged on MTR maps (357.983 ± 542.494 mm^3). As depicted in Figure 2, most of the microstructural damage at baseline was found in the lesion area (82.4 %), but it was also present in regions not related to a lesion delineated on axial T2*w (17.6 %). Finally, 25% of SC lesions identified on axial T2*w images were not associated with significant damage in MTR maps.

Location

The lesions at baseline were mainly found in WM (77.967 ± 15.234%) rather than GM. Microstructural damage in the cervical SC was also found mainly in WM regions (74.325 ± 17.853%) rather than GM. However, when lesional volume was related to GM and WM volumes, on average 5.630% (± 8.714%) of GM was affected by lesions, and 6.648% (± 8.601%) of WM. Similarly, on average, 9.824% (± 14.88%) of GM and 9.643% (± 13.13%) of WM was affected by microstructural damage. Finally, we observed a homogeneous distribution of both lesions (Fig. 5, top left) and microstructural damage (Fig. 5, top right), in terms of distance from external CSF.

####################

 # Insert Figure 2

####################

Microstructural damage and repair at 12-month follow-up

Group-level analysis

No significant difference in MTR in cervical SC was observed in pwMS between baseline (34.649 ± 2.208 pu) and 12-month follow-up (34.466 ± 2.216 pu; p = .417; Cohen's d = 0.633).

Individual-level analysis

Heterogeneity was observed in microstructural change in cervical SC over the 12-month follow-up, with values ranging from 0 to 31% for the index of dynamic microstructural damage, and 0 to 20% for the index of dynamic repair (Fig. 3, top row; see Fig. 4 for examples). The predominance profiles were also heterogeneous, with 18 patients exhibiting predominant repair, and 18 exhibiting predominant damage (no predominance in one patient) (Fig. 3, bottom left). Lesion load at baseline was positively associated with the index of dynamic damage (r = .43, p = .008), but not with either the index of dynamic repair (r = .223, p = .185) or the global index of microstructural change (r = .203, p = .228). The indices of dynamic damage (r = .506, p = .001) and repair (r = .713, p < .001) in the cervical SC were positively associated with the percentage of microstructural damage at baseline.

No association was found between any of the three indices and age or sex at baseline (all p-values > .1 after multiple comparison correction).

Five of the 37 pwMS had new lesions between C2 and C6 at 12-month follow-up. The global index of microstructural change showed predominant repair for one pwMS, and predominant damage for the other four pwMS. However, most of the microstructural damage identified at 12-month follow-up was outside the new lesions (66%).

At 12-month follow-up, 8 pwMS had a high efficacy therapy, of whom 4 had a predominance of microstructural repair, 3 of microstructural damage and 1 had no predominance.

####################

 # Insert Figure 3

####################

####################

 # Insert Figure 4

####################

Location

There was more microstructural damage over time in WM than in GM (WM/GM: 75.076/24.924 ± 14.078%). There was also more microstructural repair over time in WM than in GM (WM: 73.589/26.411 ± 19.265%). The distribution of microstructural damage (Fig. 5, bottom left) and repair (Fig 5, bottom right) over time was homogenous in terms of distance from external CSF.

####################

 # Insert Figure 5

####################

Associations with disability and atrophy measures at 5 years

Baseline microstructural damage was associated with EDSS at 5-year follow-up (r = .420, p < .001), but not with CSA change between baseline and 5-year follow-up (r = -.221, p = .063).

Similarly, baseline T2* lesion volume was associated with EDSS at 5-year follow-up (r = .340, p = .004), but not with CSA change between baseline and 5-year follow-up (r = -.144, p = .232).

The associations between the three indices and EDSS/CSA are summarised in Table 2. Positive associations were found between the index of dynamic microstructural damage and EDSS score (r = .632, p < .001), and between the global index of microstructural change and EDSS score (r = .452, p = .007) at 5-year follow-up. Furthermore, a negative association was observed between the index of dynamic microstructural damage and CSA change (r = -.416, p = .014) at 5-year follow-up. Results remained significant when baseline SC lesional volume was added as an additional covariate, and when the appearance of new lesions or number of relapses between baseline and 5-year follow-up were added as a supplementary covariate (eTable 3).

No significant group differences were found on the three indices when we compared patients with or without confirmed disability progression during follow-up (all *p*-values > .1).

######################

 # Insert Table 2

######################

Discussion

We found considerable heterogeneity in the initial extent of SC microstructural damage among pwMS. Subsequent damage/repair dynamics were also highly variable across pwMS, even for an equivalent initial lesion load. A high index of dynamic microstructural damage for the first year of the disease was associated with the development of SC atrophy at 5 years, and with an increased EDSS score, irrespective of initial SC lesion load.

Spinal cord microstructural damage at baseline

While the majority of abnormal areas on MTR were consistent with lesions detected on T2*w or on the periphery of these lesions, other areas that were farther away from the lesions only appeared abnormal on MTR *z*-score maps (Figure 2). This result can be explained by the imperfect specificity of MTR for quantifying demyelination.[8] The presence of axonal loss can also reduce MTR values,[10] affecting the lesion areas, but also having repercussions at some distance from them.[6] Moreover, the detection of SC lesions is a difficult task subject to inter-expert variability.[33] The axial T2*w sequence used in the present study had satisfactory in-plane resolution (0.7×0.7 mm²), but we cannot rule out the possibility that some small SC lesions may not have been detected. We did not find any association between distance from CSF (i.e., SC periphery) and the presence of abnormal MTR areas at baseline. In the brain, periventricular WM is known to be one of the main sites of MS lesions, as well as of lower MTR, with a gradient of values.[12,34,35] Explanatory factors include CSF proximity and the presence of pro-inflammatory factors. One potential explanation for our results is that this gradient is either weak or absent in the SC, as the latter's anatomical configuration means that it is generally close to CSF.[4]

Microstructural damage and repair at 12-month follow-up

The indices of dynamic microstructural damage and repair during the first year of the disease varied considerably across pwMS. Interestingly, we observed not only a worsening of microstructural damage in some pwMS but also an improvement in 18 pwMS. Several factors may explain these results. First, some pwMS may be able to remyelinate their SC lesions within the first year of diagnosis. Our results are consistent with previous reports concerning the variability of dynamic demyelinating/remyelinating profiles observed for brain lesions.[7,12] The limited number of pwMS included did not allow us to assess the impact of the treatments used on these profiles. Second, the MTR increase may also be due to a regression in inflammation and initial edema. However, pwMS were included more than 1 month after their most recent relapse. Third, there may have been an impact of MTR measurement variability,[20,21] given that the 19 HC were only scanned at inclusion. However, in a previous study, using the same acquisition protocol, we showed that the between-session coefficient of variation of cervical SC MTR measurement was quite small (2.0 %).[21] We also computed the indices of dynamic microstructural damage or repair on a second dataset comprising 9 HC with longitudinal SC MTR measurements acquired on another 3T MRI scanner from the same manufacturer (Siemens Prisma) (details in eAppendix 4). We found indices of damage and repair below 5 % in this HC population. Thus, the considerable variability in the indices (0-31 % and 0-21 %) for the patients in our study is probably mainly due to the effect of the pathology during follow-up.

There are probably several factors that explain the MTR decrease observed in other pwMS. First, new SC lesions may have developed. However, in 14 of 18 pwMS with a predominant microstructural damage profile, no new lesions were identified. Second, some demyelinated areas may have undergone further demyelination, as previously described in

anatomopathological studies.[4] Third, secondary axonal degeneration may have occurred. Few longitudinal studies have included quantitative SC MRI acquisitions outside acute relapse.[14,16,36] One previous study measured changes in SC MTR values at baseline, 2 years and 5 years in pwMS with more advanced disease. This study showed that a significant MTR decrease had already occurred between baseline and 2 years.[14] In our study, we failed to find a similar result, probably owing to the different profile of our population (early RRMS) and our shorter time interval (1 year). However, the observation of different early damage/repair profiles is interesting, particularly in the context of treatment developments aimed at promoting remyelination/neuroprotection.[37]

Associations with disability and atrophy measures at 5 years

A high rate of microstructural damage during the first year of the disease was associated with the development of SC atrophy and with EDSS score at 5 years, independently of the initial SC lesion load. SC lesions, particularly at an early stage of MS, are known to have a long-term prognostic value.[2,38] However, even with equal lesion load, there is substantial inter-individual variability in the development of disability.[39] Thus, the capacity of the SC microstructure to damage/repair over time is potentially an additional key factor for the development of disability. Consistent with this idea, a previous cross-sectional study showed that in patients with similar SC lesion loads, those with a high EDSS score had lower SC MTR values than those with a low EDSS score.[40] Similarly, more rapid rates of SC MTR change between baseline, 2 years and 5 years in a population of pwMS with more advanced disease were associated with increased disability at follow-up.[14] Interestingly, a previous anatomopathological study including both the brain and SC of pwMS reported a positive correlation between SC demyelination and the Multiple Sclerosis Severity Score (MSSS),[41]

as well as negative correlation between SC remyelination capacity and the MSSS.[4] No such associations were demonstrated at the cerebral level, suggesting that the extent of SC demyelination and the patient's demyelination/remyelination capacity play a prime role in the development of disability. We found an association between EDSS score at 5 years and the index of dynamic microstructural damage in our study, but no significant difference in this index between patients with or without confirmed disability progression during follow-up. This can probably be explained in part by the low baseline EDSS scores in our population (median EDSS at 0) and the known variability of EDSS measurement for these low scores. In our study, CSA was not significantly lower in patients than in HC at baseline, but the index of microstructural damage in the first year of MS was associated with CSA loss at 5 years, suggesting that microstructural damage and changes in this damage are measurable using MTR at an early stage in the disease when the CSA difference is not yet measurable, and are associated with the development of the degenerative component of the disease at 5 years. Of note, the CSA in our cohort was low compared to a recent meta-analyse.[42] Nevertheless, some studies [43,44] also reported low values when using a combination of T1w images and SCT computation, especially on Siemens scanner.

Strengths and limitations

The strengths of the present study were its prospective design, the inclusion of a homogeneous cohort of pwMS, the longitudinal MT acquisitions, and the clinical and MRI follow-up at 5 years. These features meant that we had a unique database to study the consequences of early microstructural SC damage beyond any focal lesions detected on conventional MRI. Our study nevertheless had several limitations. First, as discussed before, the variations in patients' MTR abnormalities measured between baseline and 1-year follow-up were probably linked not only to actual worsening/repair of SC microstructure, but also to

MTR measurement variability.[20,21] In particular, we did not have any reproducibility data for our MS population but believe the rather good reproducibility in HC is convincing (eAppendixes 4 and 5). Second, we used *z*-scores with a threshold of -2.58 *SD* to define an abnormal microstructure at the voxel scale in each pwMS compared with HC. To ensure that our results were not dependent on the chosen threshold, they were confirmed using a lower threshold (1.96 SD; eAppendix 3). Third, our study had a rather small sample size and confirmation with a larger cohort is needed. Fourth, as discussed above, MTR has limited specificity for myelin content or axonal loss. Our findings therefore need to be confirmed using other myelin-sensitive imaging techniques such as T1w [35,45] or T2w relaxometry,[46,47] MTSat[48] or ihMT,[49] and other axon-sensitive diffusion models,[50,51] although none of these techniques has perfect specificity.[52] Finally, it would be particularly interesting to replicate our study using sequences with shorter acquisition time and therefore compatible with clinical use, such as MP2RAGE.[53]

Conclusion and perspectives

Our study suggests that a high index of dynamic microstructural damage in the SC of people with early RRMS is associated with greater development of SC atrophy at 5 years, and an increased EDSS score, irrespective of initial SC lesion load. Further imaging studies that accurately describe the dynamics of SC demyelination and axonal loss in pwMS are needed to confirm our results, better understand the substrate of progressive ambulatory disability, and test the effects of new treatments on this damage.

Acknowledgments

We are grateful for the tremendous efforts made by all EMISEP study teams across participating sites. Furthermore, we express our sincere gratitude to all the volunteers and

their family members who are participating in the EMISEP study. We gratefully acknowledge all the administrative, medical and scientific staff members involved in data acquisition, data management, and quality control. We would like to thank Elizabeth Portier and Ricky Walsh for checking the English style. MRI data acquisition was supported by the Neurinfo MRI research facility from the University of Rennes I, University Hospital of Rennes, Inria, CNRS and the Rennes Cancer Center. Neurinfo was also supported by the European Research Council (FEDER), the French State, the Brittany Council, Rennes Metropole, Inserm and GIS IBISA

Funding information

This research was supported by the French Hospital Programme of Clinical Research (PHRC).

Competing interests

The authors report no competing interests in relation to the work described here.

Author contributions

Conception of the study and acquisition of the data: BC, EB, JCF, LM, ELP, GE, AK

Analyses of the present data: MG, BC, EB, AM, VC, GB, BS, BB, AK

Interpretation of the present data: MG, BC, EB, BB, AK

Manuscript drafting and/or revision: MG, BC, EB, ELP, BB, AK

All authors contributed to the article and approved the final version.

References

1. Bot JCJ, Barkhof F, Polman CH, et al. Spinal cord abnormalities in recently diagnosed MS patients: added value of spinal MRI examination. Neurology. 2004;62:226–233.

2. Brownlee WJ, Altmann DR, Prados F, et al. Early imaging predictors of long-term outcomes in relapse-onset multiple sclerosis. Brain. 2019;142:2276–2287.

3. Gilmore CP, Geurts JJG, Evangelou N, et al. Spinal cord grey matter lesions in multiple sclerosis detected by post-mortem high field MR imaging. Mult Scler. 2009;15:180–188.

4. Bramow S, Frischer JM, Lassmann H, et al. Demyelination versus remyelination in progressive multiple sclerosis. Brain. 2010;133:2983–2998.

5. Bjartmar C, Kidd G, Mörk S, Rudick R, Trapp BD. Neurological disability correlates with spinal cord axonal loss and reduced N-acetyl aspartate in chronic multiple sclerosis patients. Ann Neurol. Wiley; 2000;48:893–901.

6. Petrova N, Carassiti D, Altmann DR, Baker D, Schmierer K. Axonal loss in the multiple sclerosis spinal cord revisited. Brain Pathol. 2018;28:334–348.

7. Bodini B, Veronese M, García-Lorenzo D, et al. Dynamic I maging of I ndividual R emyelination P rofiles in M ultiple S clerosis. Ann Neurol. Wiley; 2016;79:726–738.

8. Schmierer K, Scaravilli F, Altmann DR, Barker GJ, Miller DH. Magnetization transfer ratio and myelin in postmortem multiple sclerosis brain. Ann Neurol. 2004;56:407–415.

9. Gareau PJ, Rutt BK, Karlik SJ, Mitchell JR. Magnetization transfer and multicomponent T2 relaxation measurements with histopathologic correlation in an experimental model of MS. J Magn Reson Imaging. 2000;11:586–595.

10. van Waesberghe JH, Kamphorst W, De Groot CJ, et al. Axonal loss in multiple sclerosis lesions: magnetic resonance imaging insights into substrates of disability. Ann Neurol. 1999;46:747–754.

11. Chen JT, Collins DL, Atkins HL, Freedman MS, Arnold DL, Canadian MS/BMT Study Group. Magnetization transfer ratio evolution with demyelination and remyelination in multiple sclerosis lesions. Ann Neurol. 2008;63:254–262.

12. Tonietto M, Poirion E, Lazzarotto A, et al. Periventricular remyelination failure in multiple sclerosis: a substrate for neurodegeneration. Brain. 2023;146:182–194.

13. Lazzarotto A, Hamzaoui M, Tonietto M, et al. Time is myelin: early cortical myelin repair prevents atrophy and clinical progression in multiple sclerosis. Brain. 2024;147:1331–1343.

14. Oh J, Chen M, Cybulsky K, et al. Five-year longitudinal changes in quantitative spinal cord MRI in multiple sclerosis. Mult Scler. 2021;27:549–558.

15. Freund P, Wheeler-Kingshott C, Jackson J, Miller D, Thompson A, Ciccarelli O. Recovery after spinal cord relapse in multiple sclerosis is predicted by radial diffusivity. Mult Scler. 2010;16:1193–1202.

16. Agosta F, Absinta M, Sormani MP, et al. In vivo assessment of cervical cord damage in MS patients: a longitudinal diffusion tensor MRI study. Brain. 2007;130:2211–2219.

17. Théaudin M, Saliou G, Ducot B, et al. Short-term evolution of spinal cord damage in multiple

sclerosis: a diffusion tensor MRI study. Neuroradiology. 2012;54:1171–1178.

18. Ciccarelli O, Altmann DR, McLean MA, et al. Spinal cord repair in MS: does mitochondrial metabolism play a role? Neurology. 2010;74:721–727.

19. Bellenberg B, Busch M, Trampe N, Gold R, Chan A, Lukas C. 1H-magnetic resonance spectroscopy in diffuse and focal cervical cord lesions in multiple sclerosis. Eur Radiol. 2013;23:3379–3392.

20. Lévy S, Guertin M-C, Khatibi A, et al. Test-retest reliability of myelin imaging in the human spinal cord: Measurement errors versus region- and aging-induced variations. PLoS One. 2018;13:e0189944.

21. Combès B, Monteau L, Bannier E, et al. Measurement of magnetization transfer ratio (MTR) from cervical spinal cord: Multicenter reproducibility and variability. J Magn Reson Imaging. 2019;49:1777–1785.

22. Polman CH, Reingold SC, Banwell B, et al. Diagnostic criteria for multiple sclerosis: 2010 revisions to the McDonald criteria. Ann Neurol. 2011;69:292–302.

23. Kurtzke JF. Rating neurologic impairment in multiple sclerosis: an expanded disability status scale (EDSS). Neurology. 1983;33:1444–1452.

24. Goldman MD, Marrie RA, Cohen JA. Evaluation of the six-minute walk in multiple sclerosis subjects and healthy controls. Mult Scler. 2008;14:383–390.

25. Cutter GR, Baier ML, Rudick RA, et al. Development of a multiple sclerosis functional composite as a clinical trial outcome measure. Brain. 1999;122 (Pt 5):871–882.

26. Hobart JC, Riazi A, Lamping DL, Fitzpatrick R, Thompson AJ. Measuring the impact of MS on walking ability: the 12-Item MS Walking Scale (MSWS-12). Neurology. 2003;60:31–36.

27. Bonniaud V, Parratte B. [Cross-cultural adaptation of health-related quality of life questionnaire: English version of Qualiveen abstract]. Ann Readapt Med Phys. 2006;49:92–99.

28. De Leener B, Lévy S, Dupont SM, et al. SCT: Spinal Cord Toolbox, an open-source software for processing spinal cord MRI data. Neuroimage. 2017;145:24–43.

29. Jenkinson M, Beckmann CF, Behrens TEJ, Woolrich MW, Smith SM. FSL. Neuroimage. 2012;62:782–790.

30. Website [online]. Accessed at: https://anima.irisa.fr,.

31. De Leener B, Fonov VS, Collins DL, Callot V, Stikov N, Cohen-Adad J. PAM50: Unbiased multimodal template of the brainstem and spinal cord aligned with the ICBM152 space. Neuroimage. 2018;165:170–179.

32. Combès B, Kerbrat A, Ferré JC, et al. Focal and diffuse cervical spinal cord damage in patients with early relapsing–remitting MS: A multicentre magnetisation transfer ratio study. Mult Scler. SAGE Publications Ltd STM; 2019;25:1113–1123.

33. Gros C, De Leener B, Badji A, et al. Automatic segmentation of the spinal cord and intramedullary multiple sclerosis lesions with convolutional neural networks. Neuroimage. 2019;184:901–915.

34. Poirion E, Tonietto M, Lejeune F-X, et al. Structural and Clinical Correlates of a Periventricular Gradient of Neuroinflammation in Multiple Sclerosis. Neurology. 2021;96:e1865–e1875.

35. Kolb H, Absinta M, Beck ES, et al. 7T MRI Differentiates Remyelinated from Demyelinated Multiple Sclerosis Lesions. Ann Neurol. 2021;90:612–626.

36. Laule C, Vavasour IM, Zhao Y, et al. Two-year study of cervical cord volume and myelin water in primary progressive multiple sclerosis. Mult Scler. 2010;16:670–677.

37. Lubetzki C, Zalc B, Williams A, Stadelmann C, Stankoff B. Remyelination in multiple sclerosis: from basic science to clinical translation. Lancet Neurol. 2020;19:678–688.

38. Arrambide G, Rovira A, Sastre-Garriga J, et al. Spinal cord lesions: A modest contributor to diagnosis in clinically isolated syndromes but a relevant prognostic factor. Mult Scler. 2018;24:301–312.

39. Barkhof F. The clinico-radiological paradox in multiple sclerosis revisited [online]. Current Opinion in Neurology 2002. p. 239–245. Accessed at: http://dx.doi.org/10.1097/00019052-200206000-00003.

40. Oh J, Saidha S, Chen M, et al. Spinal cord quantitative MRI discriminates between disability levels in multiple sclerosis. Neurology. 2013;80:540–547.

41. Roxburgh RHSR, Seaman SR, Masterman T, et al. Multiple Sclerosis Severity Score: using disability and disease duration to rate disease severity. Neurology. 2005;64:1144–1151.

42. Trolle C, Goldberg E, Linnman C. Spinal cord atrophy after spinal cord injury - A systematic review and meta-analysis. Neuroimage Clin. 2023;38:103372.

43. Cohen-Adad J, Alonso-Ortiz E, Abramovic M, et al. Open-access quantitative MRI data of the spinal cord and reproducibility across participants, sites and manufacturers. Sci Data. 2021;8:219.

44. Lukas C, Bellenberg B, Prados F, et al. Quantification of Cervical Cord Cross-Sectional Area: Which Acquisition, Vertebra Level, and Analysis Software? A Multicenter Repeatability Study on a Traveling Healthy Volunteer. Front Neurol. 2021;12:693333.

45. Demortière S, Lehmann P, Pelletier J, Audoin B, Callot V. Improved Cervical Cord Lesion Detection with 3D-MP2RAGE Sequence in Patients with Multiple Sclerosis. AJNR Am J Neuroradiol. 2020;41:1131–1134.

46. Dvorak AV, Ljungberg E, Vavasour IM, et al. Rapid myelin water imaging for the assessment of cervical spinal cord myelin damage [online]. NeuroImage: Clinical 2019. p. 101896. Accessed at: http://dx.doi.org/10.1016/j.nicl.2019.101896.

47. Lee LE, Vavasour IM, Dvorak A, et al. Cervical cord myelin abnormality is associated with clinical disability in multiple sclerosis. Mult Scler. 2021;27:2191–2198.

48. Lema A, Bishop C, Malik O, et al. A Comparison of Magnetization Transfer Methods to Assess Brain and Cervical Cord Microstructure in Multiple Sclerosis. J Neuroimaging. Wiley Online Library; 2017;27:221–226.

49. Rasoanandrianina H, Demortière S, Trabelsi A, et al. Sensitivity of the Inhomogeneous Magnetization Transfer Imaging Technique to Spinal Cord Damage in Multiple Sclerosis. AJNR Am J Neuroradiol. 2020;41:929–937.

50. Assaf Y, Freidlin RZ, Rohde GK, Basser PJ. New modeling and experimental framework to characterize hindered and restricted water diffusion in brain white matter. Magn Reson Med. 2004;52:965–978.

51. Alexander DC, Hubbard PL, Hall MG, et al. Orientationally invariant indices of axon diameter and density from diffusion MRI. Neuroimage. 2010;52:1374–1389.

52. Granziera C, Wuerfel J, Barkhof F, et al. Quantitative magnetic resonance imaging towards clinical application in multiple sclerosis. Brain. 2021;144:1296–1311.

53. Forodighasemabadi A, Rasoanandrianina H, El Mendili MM, Guye M, Callot V. An optimized MP2RAGE sequence for studying both brain and cervical spinal cord in a single acquisition at 3T. Magn Reson Imaging. 2021;84:18–26.

Tables

Table 1: ***Participant's Demographic and Clinical Characteristics.***

	HC (*n* = 19)	**RRMS (*n* = 37)**		**HC vs. RRMS at baseline *p* value**	**RRMS at baseline vs. 5-year follow-up *p* value**
		Baseline (*n* = 37)	**5-year follow-up (*n* = 36)**		
Sex, % male	52.63	35.13		.208	
Age at first MRI, years	32.58 (8.18)	32.24 (5.89)		.861	
Age at RRMS diagnosis, years		31.60 (5.85)			
Time between baseline MRI and 12-month follow-up, years		0.90 (0.15)			
Time between baseline MRI and 5-year follow-up, years		5.06 (0.26)			
Treatment at baseline, % (n)					
Medium efficacy therapy		95.6 (35)	48.6 (18)		
High efficacy therapy		2.7 (1)	45.9 (17)		
No treatment		2.7 (1)	2.7 (1)		
EDSS		0.00 [0.00, 2.50]	1.00 [0.00, 7.50]		.193
Pyramidal EDSS		0.00 [0.00, 2.00]	0.00 [0.00, 4.00]		.109
T25-FW, minutes		4.60 [2.75, 6.30]	4.70 [3.30, 6.08]		.749

	HC (n = 19)	RRMS (n = 37)		HC vs. RRMS at baseline p value	RRMS at baseline vs. 5-year follow-up p value
		Baseline (n = 37)	5-year follow-up (n = 36)		
Sex, % male	52.63	35.13		.208	
Age at first MRI, years	32.58 (8.18)	32.24 (5.89)		.861	
Age at RRMS diagnosis, years		31.60 (5.85)			
76MWT, metres		510.00 [396.00, 792.00]	504.50 [0.00, 715.00]		.416
1/9HPT		0.05 [0.03, 0.06]	0.06 [0.03, 0.07]		<.001
MSWS-12		12.00 [12.00, 53.00]	12.00 [12.00, 60.00]		.368
Qualiveen		0.00 [0.00, 1.06]	0.00 [0.00, 2.85]		.372
CSA, mm²	59.72 (5.6)	62.917 (6.294)	58.832 (7.54)	.166	<.001

Note: Data are shown as means (± standard deviation), or medians [range] for clinical scores, unless stated otherwise. Two-sample t *tests were used for age and CSA comparisons between the healthy group (HC) and relapsing-remitting multiple sclerosis (RRMS) groups, and* χ^2 *for sex ratio comparisons. For clinical scores, paired* t *tests were computed to compare baseline and 5-year follow-up in patients with RRMS. EDSS: Expanded Disability Status Scale, T25-FW: 8-metres timed-walked, 6M-walk: 6-minutes walk, 9HPT: nine holes peg test, MSWS-12: twelve item MS walking scale, Qualiveen: urinary quality of life questionnaire, CSA: cross-sectional area. Data for the T25-FW test was missing for one RRMS patient at 5-year follow-up as this patient was no longer able to walk.*

Table 2: ***Results of Multiple Regressions Between Expanded Disability Status Scale (EDSS) and Cross-Sectional Area (CSA) Change at 5-Year Follow-Up and the Three Indices of Dynamic Microstructural Change Between Baseline and 12-Month Follow-Up.***

	Multiple regression with age and sex as covariates		**Multiple regression with age, sex, and T2*w spinal cord lesion load as covariates**	
	r	***p* value**	***r***	***p* value**
EDSS at 5-year follow-up				
Index of dynamic microstructural damage	.632	< .001*	.603	< .001*
Index of dynamic microstructural repair	.051	.774	.018	.920
Global index of microstructural change	.452	.007*	.43	.0126*
CSA change between baseline and 5-year follow-up				
Index of dynamic microstructural damage	-.416	.014*	-.399	.021*
Index of dynamic microstructural repair	-.176	.319	-.161	.372
Global index of microstructural change	-.202	.251	-.184	.305

*Note. Results are displayed with age and sex (lefthand columns) and age, sex, and T2*w lesion load (righthand columns) as covariates. *:* $p < .05$. *P-values that survived Bonferroni correction are underlined.*

Figure legends

Figure 1: Schematic overview of computation of the three dynamic indices. First, baseline (BL) and 12-month follow-up (12M-FU) magnetisation transfer ratios were normalised (and smoothed) to PAM50 space, and z-score maps were computed based on means and standard deviations (SD) from the HC group (A). Then, the two z-score maps were binarised at -2.58 SD and merged into a single map displaying damage at baseline only (blue), follow-up only (yellow), or both (purple) (B). Finally, the three indices used in the study were calculated (C).

Figure 2: Examples of five patients with relapsing-remitting multiple sclerosis with different degrees of lesion load (blue) and microstructural damage (orange), and the intersection between the two (green), in cervical spinal cord at baseline. The second line displays the raw z-score maps of the corresponding five patients. On top are displayed the distance from the centre of the spinal cord from left to right.

Figure 3. Changes in microstructural damage changes between baseline and 12-month follow-up in cervical SC of individual patients: index of dynamic microstructural damage *(top left), index of dynamic* microstructural repair *(top right), global index of* microstructural *change (bottom left), and lesion load at baseline (bottom right). All graphs are ordered according to the global index of* microstructural *change values.*

*Figure 4: Examples of two patients with relapsing-remitting multiple sclerosis with a high T2*w lesion load and exhibited profiles of either predominant microstructural damage (left) or predominant microstructural repair (right) over time. For each patient, the T2*w lesions are displayed on the left (green), while microstructural damage and repair over time are*

displayed on the right. The left part of the figure shows the sagittal view of the PAM50 T2 and the level of the different axial slices.

Figure 5: Relationships between baseline and follow-up indices with external cerebrospinal fluid (CSF). Lesion load (%) at baseline (graph top left), microstructural damage at baseline (graph top right), microstructural damage over time (graph bottom left), and microstructural repair over time (graph bottom right), according to distance from external CSF. Median, interquartile range, and overall range are represented in the boxplots, and means are shown as solid circles. Figures map the distance between external CSF (cool colours) and the centre of the spinal cord (hot colours).

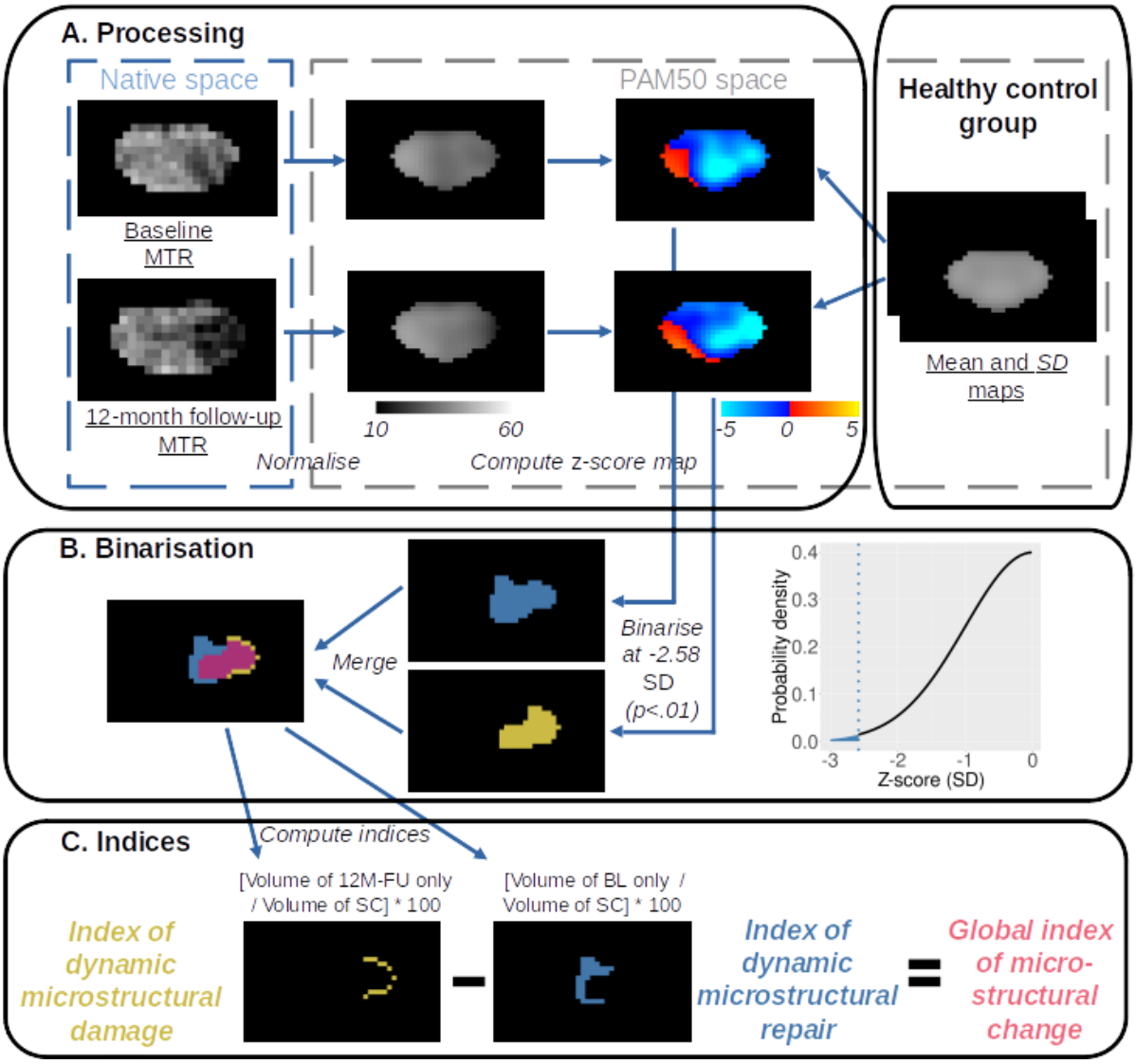

Figure 1: ***Schematic overview of computation of the three dynamic indices****. First, baseline (BL) and 12-month follow-up (12M-FU) magnetisation transfer ratios were normalised (and smoothed) to PAM50 space, and z-score maps were computed based on means and standard deviations (SD) from the HC group (A). Then, the two z-score maps were binarised at -2.58 SD and merged into a single map displaying damage at baseline only (blue), follow-up only (yellow), or both (purple) (B). Finally, the three indices used in the study were calculated (C).*

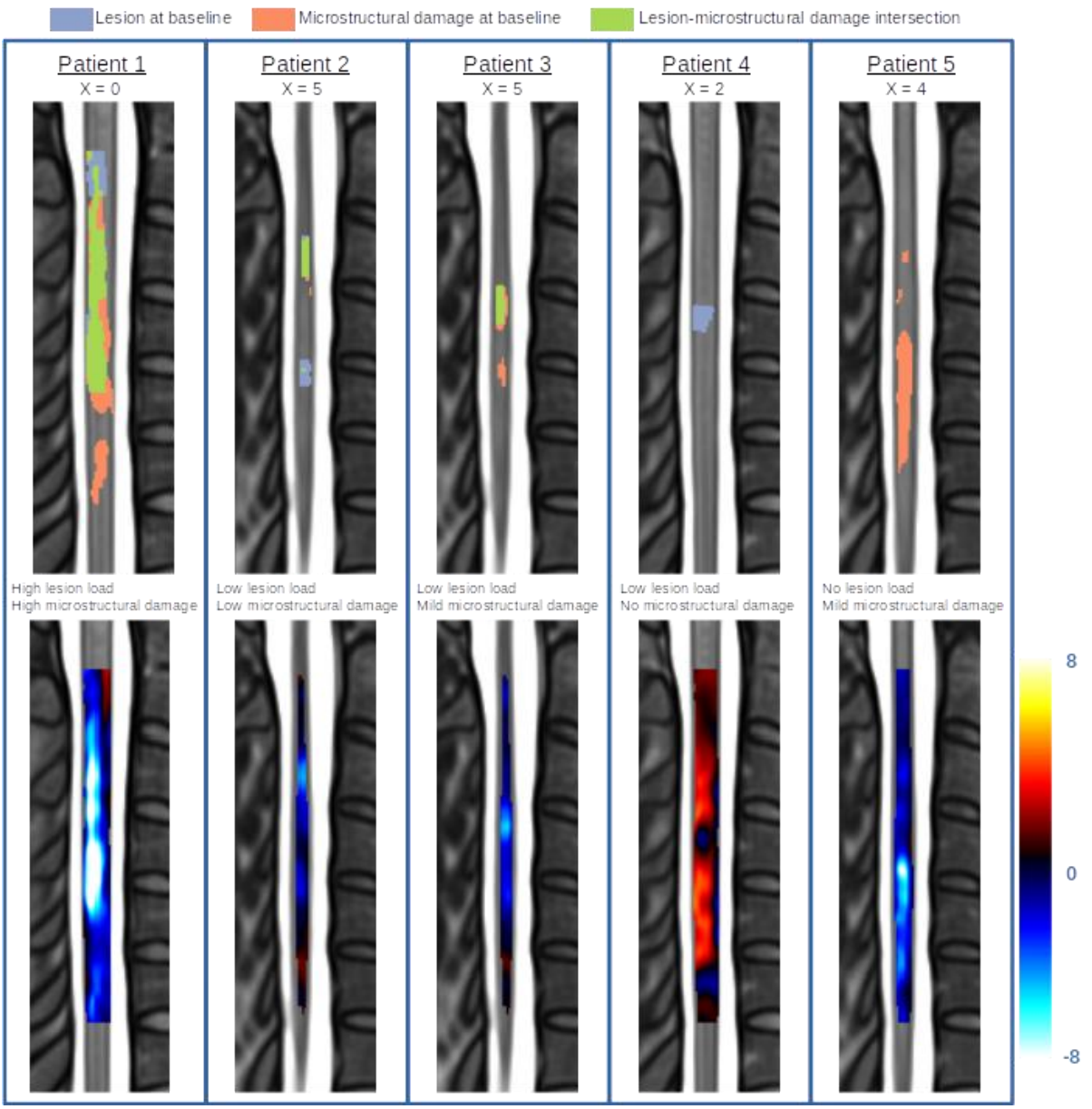

Figure 2: ***Examples of five patients with relapsing-remitting multiple sclerosis with different degrees of lesion load (blue) and microstructural damage (orange), and the intersection between the two (green), in cervical spinal cord at baseline****. The second line displays the raw z-score maps of the corresponding five patients. On top are displayed the distance from the centre of the spinal cord from left to right.*

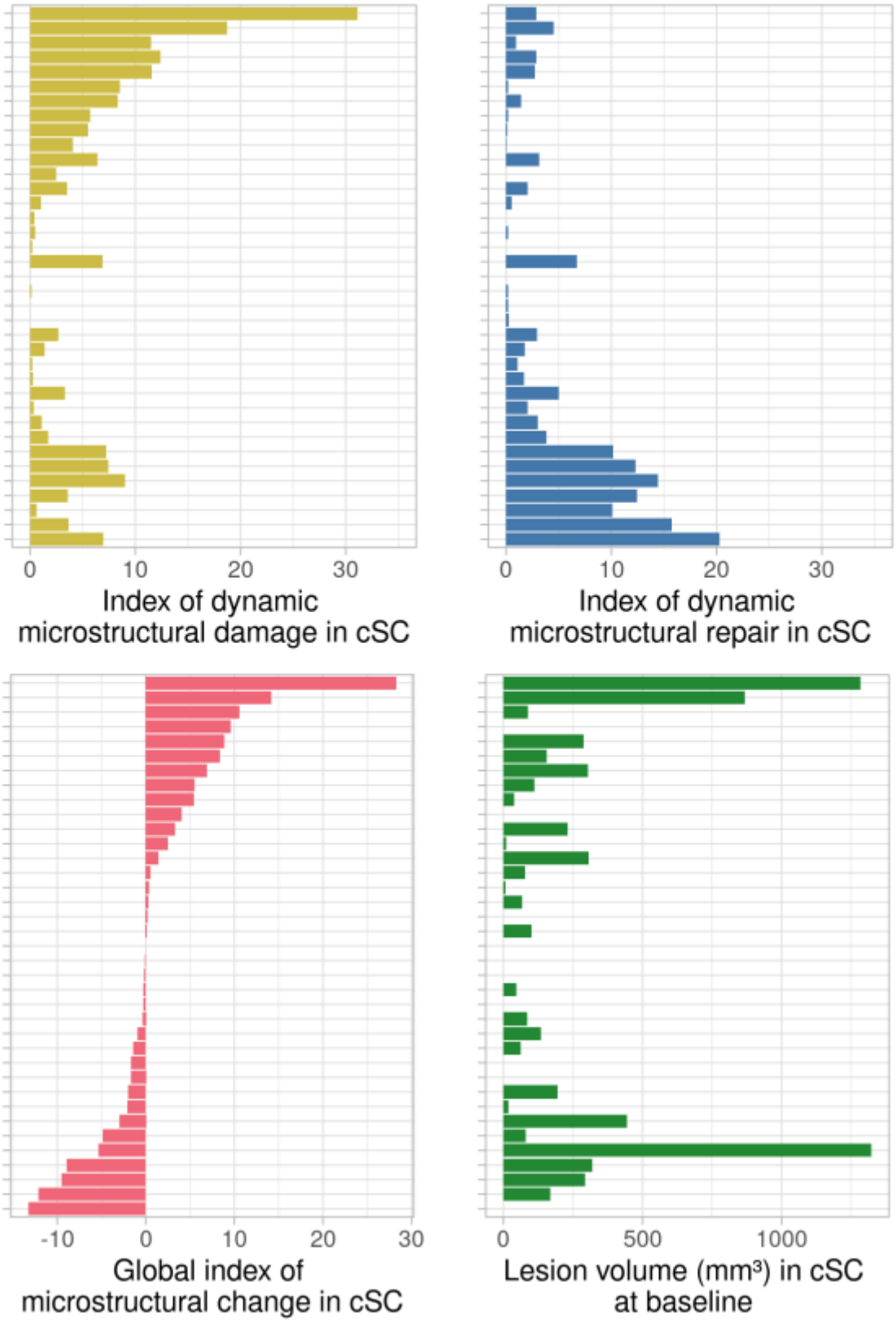

Figure 3. ***Changes in microstructural damage changes between baseline and 12-month follow-up in cervical SC of individual patients****: index of dynamic* microstructural damage

(top left), index of dynamic microstructural repair *(top right), global index of* microstructural *change (bottom left), and lesion load at baseline (bottom right). In each graph, each bar represents one subject. All graphs are ordered according to the global index of* microstructural *change values.*

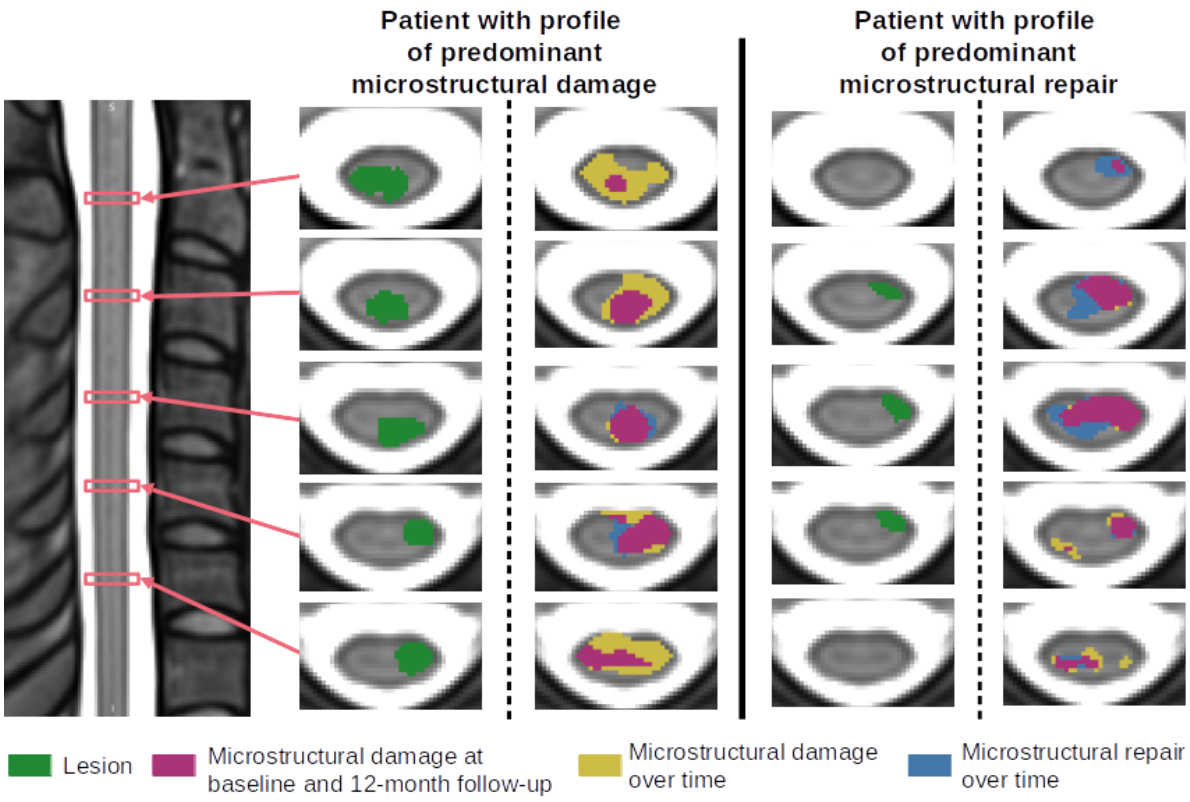

Figure 4: ***Examples of two patients with relapsing-remitting multiple sclerosis with a high T2*w lesion load and exhibited profiles of either predominant microstructural damage (left) or predominant microstructural repair (right) over time****. For each patient, the T2*w lesions are displayed on the left (green), while microstructural damage and repair over time are displayed on the right. The left part of the figure shows the sagittal view of the PAM50 T2 and the level of the different axial slices.*

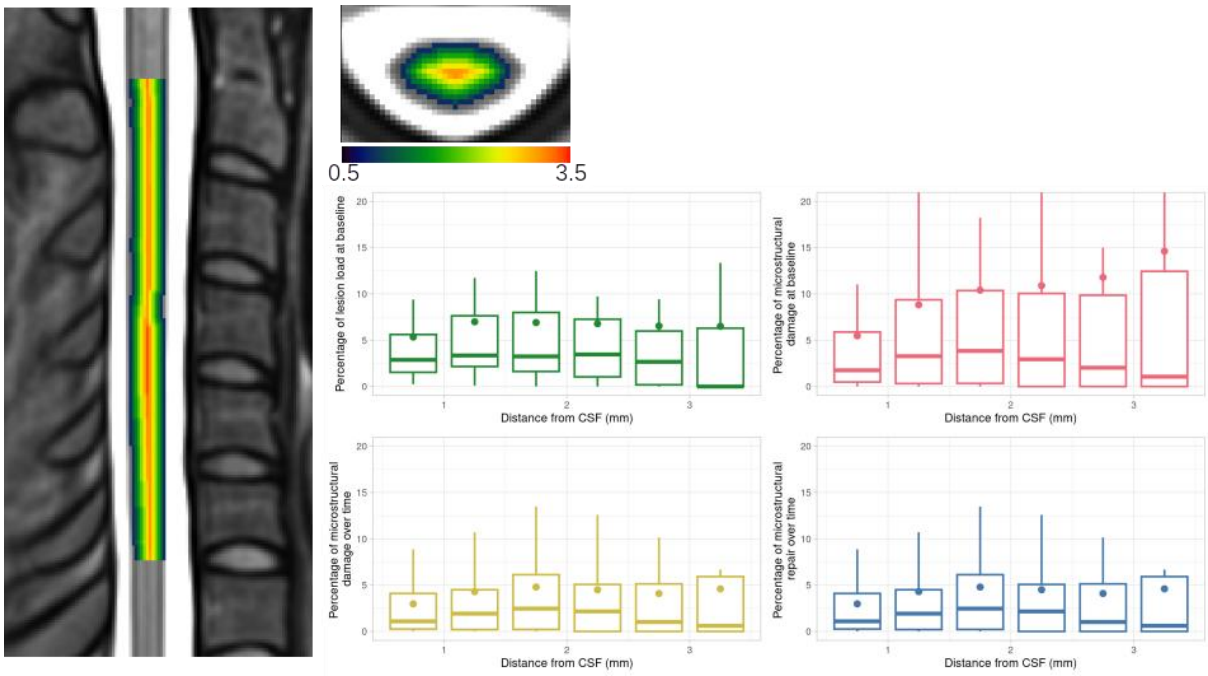

Figure 5: ***Relationships between baseline and follow-up indices with external cerebrospinal fluid (CSF).*** *Lesion load (%) at baseline (graph top left), microstructural damage at baseline (graph top right), microstructural damage over time (graph bottom left), and microstructural repair over time (graph bottom right), according to distance from external CSF. Median, interquartile range, and overall range are represented in the boxplots, and means are shown as solid circles. Figures map the distance between external CSF (cool colours) and the centre of the spinal cord (hot colours).*